Denitrifying bradyrhizobia retain strong N_2O reduction during periods of starvation

Yuan Gao, Magnus Øverlie Arntzen, Morten Kjos, Lars R. Bakken and Åsa Frostegård

Faculty of Chemistry, Biotechnology and Food Sciences, Norwegian University of Life Sciences, N-1432 Ås, Norway

Abstract

Rhizobia living as microsymbionts inside nodules have stable access to carbon substrates, but also have to survive as free-living bacteria in soil where they are starved for carbon and energy most of the time. Many rhizobia can denitrify, thus switch to anaerobic respiration under low O_2 tension using N-oxides as electron acceptors. The cellular machinery regulating this transition is relatively well-known from studies under optimal laboratory conditions, while little is known about this regulation in starved organisms. It is, for example, not known if the strong preference for N_2O- over NO_3^--reduction in bradyrhizobia is retained under carbon limitation. Here we show that starved cultures of a *Bradyrhizobium* strain with respiration rates 1-18% of well-fed cultures, reduced all available N_2O before touching provided NO_3^-. Proteomics showed similar abundance of Nap (periplasmic NO_3^- reductase) and NosZ (N_2O reductase), suggesting that competition between electron pathways to Nap and NosZ favoured N_2O reduction also in starved cells, similar to well-fed cultures. This contrasts the general notion that NosZ activity diminishes under carbon limitation. The results suggest that bradyrhizobia carrying NosZ can act as strong sinks for N_2O under natural conditions and that this criterion should be considered in the development of biofertilizers.

Importance

Novel biotechnological approaches are needed to curb the escalating emissions of the greenhouse gas N_2O from agricultural soils. One possibility is inoculation of N_2O-reducing organisms into soil. Rhizobial inoculants are used at large scale to enhance N_2-fixation of legumes. The genus *Bradyrhizobium* encompasses N_2-fixing symbionts of economically important legumes. Most bradyrhizobia can also denitrify, but the commercially available inoculants generally lack the last denitrification step, reduction of N_2O. Recent results revealed that bradyrhizobia with complete denitrification strongly favor N_2O over nitrate, making them potential strong sinks for N_2O. In those studies the cultures received ample amounts of substrate, while bacteria in soil generally starve. Here we demonstrate that bradyrhizobia retain their strong preference for N_2O also under carbon starvation. The findings add basic knowledge about mechanisms controlling denitrification and support the potential for developing new bradyrhizobial legume inoculants with the dual capacity to optimize N_2-fixation and minimize N_2O emission.

Introduction

Bacteria in most natural and engineered environments are faced with fluctuating availability of nutrients and need to adapt to a “feast and famine” lifestyle. While many soil types are rich in total organic carbon, the concentration of bioavailable carbon substrate is low, particularly in non-rhizosphere soil where lack of substrate is a major factor limiting the growth of heterotrophic bacteria (1). It is likely that bacteria in soil are starved most of the time (2) and only experience infrequent episodes of ample provision of carbon substrate, for example as

exudates from a root or organic material released during decay of dead (micro)organisms. Bacteria have developed several strategies to survive extended periods of starvation, such as the development of high-affinity uptake systems to scavenge alternative carbon sources from the surroundings, as well as changes in cell morphology, condensation of the nucleoid and decreased protein synthesis to adapt to a low metabolic activity (3). Many bacteria produce carbon-rich storage materials such as PHA (poly-3-hydroxyalkanoates) and glycogen during periods of substrate availability, which can be utilized to sustain a minimum of metabolic activity when deprived of carbon and energy (4,5).

Several of the microbially mediated processes in the global nitrogen cycle are closely linked to the carbon (C) metabolism of the organisms. One example is denitrification, which is the reduction of NO_3^- to N_2 through anaerobic respiration where the N-oxides are used as terminal electron acceptors when O_2 becomes scarce. This process can be performed by a diverse range of heterotrophic bacteria, archaea and fungi, which use various forms of organic compounds as electron donors to obtain energy (6) or, in some cases, H_2 (7). The last step of denitrification is the reduction of N_2O, a strong climate gas, to harmless N_2, catalyzed by the N_2O reductase (Nos) (8,9). It is found in a diverse range of prokaryotic organisms but has not been reported in eukaryotes. Some denitrifying prokaryotes can perform all steps of denitrification, others only some, and lack of the last step is common due to absence of the *nosZ* gene coding for NosZ , or lack of other essential gene(s) in the *nos* operon (10,11), but the amounts of N_2O released from denitrification in relation to N_2 (the N_2O/N_2 product ratio) is also influenced by transcriptional and post-transcriptional control mechanisms and by various environmental factors (6,12-19). Denitrification in agricultural soils is a major source of N_2O, accounting for more than 60% of

the global anthropogenic emissions (20,21). A steady increase in atmospheric N_2O has been recorded since the start of industrialization, largely driven by increasing and excessive use of synthetic fertilizers (22,23) and these emissions are predicted to continue to increase unless novel mitigation options are developed (24,25).

Although the addition of reactive nitrogen compounds via synthetic fertilizers accounts for the main part of the N_2O emissions from agricultural soil, the N_2O emitted from legume cropped fields is far from negligible. A compilation of data from ca 70 legume cropped fields estimated ca 1.29 kg N_2O-N ha^{-1} during one growing season, while the corresponding data for N-fertilized crops and pastures showed emissions of 3.22 kg N_2O-N ha^{-1} (26). Legumes do not have to rely on uptake of reactive N such as NH_4^+ or NO_3^- but can acquire N through their symbiotic relationship with some groups of bacteria, collectively called rhizobia, that elicit the production of root nodules on the plant in which they fix atmospheric N_2. In this process, the rhizobia reduce N_2 to NH_3 and the plant cells reduce the NH_3 further to glutamine which they use to produce amino acids and eventually proteins (27). When this N-rich plant material is degraded, organic N is released and mineralized to NH_3/NH_4^+ which will be oxidized to NO_3^- by nitrifying organisms. The O_2 consumption by the nitrifiers, together with the production of NO_3^- and the availability of organic compounds from the degraded plants, creates conditions that are conducive to denitrification. A novel approach to minimize N_2O emissions from agricultural soil is to enhance the populations of N_2O reducing bacteria (25). In the case of legume crops, which are often inoculated with rhizobia to optimize the N_2-fixation, there are a few promising studies reporting decreased N_2O emissions from soybean fields inoculated with rhizobia with the dual capability of efficient N_2 fixation and N_2O reduction (28,29).

89 Based on this, selection of rhizobial strains for development of commercial inoculants
90 should, ideally, take both these aspects into account. One problem is, however, that far from all
91 rhizobia carry the *nosZ* gene that encodes Nos. There are relatively few surveys of
92 denitrification genes in different groups of rhizobia. Complete denitrification, which includes all
93 four reduction steps of NO_3^- to N_2, has so far mainly been reported for the genus
94 *Bradyrhizobium*, which is the microsymbiont of a range of economically important legume
95 crops such as soybean, cow pea and peanut (30,31). A full set of denitrification reductases in
96 bradyrhizobia include, with few exceptions, the periplasmic NO_3^- reductase Nap; the Cu-
97 containing NO_2^- reductase NirK, the *bc*-type NO reductase cNor and a NosZ belonging to clade I
98 (19,32). We recently investigated the denitrification capacity of bradyrhizobia from two strain
99 collections, one obtained from nodules of legume trees and herbs growing in Ethiopia, the
100 other mainly consisting of strains isolated from nodules of peanut growing in China (18,19). In
101 these collections, 50 and 37% of the isolates, respectively, were complete denitrifiers, while the
102 others generally lacked NosZ and thus were potential N_2O sources. Common to all strains with
103 complete denitrification was a strong preference for N_2O- over NO_3^- reduction. Transcription
104 analysis and proteomics showed comparable expression levels of Nap and Nos, suggesting a
105 control mechanism at the metabolic level where the electron pathway to Nos, which receives
106 electrons from cytochrome *c* via the *bc1* complex, competes very efficiently with the electron
107 pathway to Nap which goes via the membrane bond NapC.
108 The results presented in (18,19) were based on experiments with organisms provided with
109 ample amounts of C substrate (electron donor), which is likely to reflect the situation in legume
110 nodules where the microsymbiont receives C from the plant. It can, however, be expected that

rhizobia, which may survive for many years in soil (33), spend a large part of their life cycle as free-living organisms in soil where they will experience lack of available C substrate most of the time (2). Rhizobial inoculants that carry NosZ are thus potentially important sinks for N_2O produced both by themselves and by other soil microbes. It is, however, not known if the competition for electrons favoring N_2O reduction in well-fed cultures is retained during substrate limitation ("starvation"). Here we exposed cultures of *Bradyrhizobium* strain HAMBI 2125, also studied in (19), to shorter and extended periods of starvation and analyzed the denitrification kinetics, including the electron flow rates to the individual denitrification reductases. We also quantified the cellular abundancies of Nap, Nir and Nos. The results have practical implications, supporting that these organisms can act as sinks for N_2O under natural conditions. Moreover, the results are ecologically interesting since they show that cultures exposed to extended starvation divided into two opposite denitrification phenotypes, one with very slow metabolism, the other with retained metabolism, possibly reflecting a strategy to increase the chances for survival during periods of starvation.

Results

Denitrification kinetics in cultures prepared following Bioassay 1. Two bioassays were developed for starvation experiments, Bioassay 1 and 2 (Figs. 1A and B). In a first experiment, the denitrification gas kinetics, concentrations of NO_3^- and NO_2^- and electron flow rates to the different reductases were compared for well-fed *vs* starved cultures (Figs. 2A-D). For this, the starved cultures were prepared following Bioassay 1 (Fig. 1A), in which the cultures were allowed to synthesize the denitrification reductases in the presence of ample amounts of

133 substrate. Cultures were raised under fully oxic conditions in YMB medium, after which the
134 headspace was made hypoxic to allow transition to anaerobic respiration in response to a
135 gradual depletion of oxygen. After centrifugation/washing, pellets were pooled and inoculated
136 into flasks containing YMB (9.9E+08 cells flask^{-1}) or buffer (5.0E+09 cells flask^{-1}), supplemented
137 with 1 mM KNO_3 and 0.25 mM KNO_2, and with He plus 1 ml N_2O (around 80 µmol N) in
138 headspace.

139 The initial O_2 concentration, which was 0.5 µM in cultures with YMB and 0.2 µM in cultures
140 with buffer, was depleted within the first 5 h in both treatments (insets in Figs. 2A and B). The
141 provided NO_2^- and N_2O were reduced simultaneously from the beginning of the incubation in
142 both treatments. The NO_3^- was left untouched in the well-fed cultures until the exogenous N_2O
143 was reduced (Fig. 2A), also seen from lack of electron flow to Nap except for a small peak in
144 electron flow early in the anoxic incubation (Fig. 2C). No NO_3^- reduction took place in the
145 starved cultures throughout the entire incubation period, as seen from the lack of electron flow
146 to Nap (Fig. 2D). The negative V_{eNap} estimated for the starved cultures (inset in Fig. 2D) and the
147 initial phase of the well-fed cultures are probably due to minor errors in calibration of N-gas
148 measurements as well as in parameters used to calculate rates of N-transformation (sampling
149 loss and N_2-leakage, see Molstad et al. (34)), which amounts to substantial errors in the
150 estimates of NO_3^-reduction rates because they are based on N-mass balance (explained in detail
151 by Lim et al. (35)). This implies a relatively high detection limit for NO_3^- reduction, and the
152 negative values cannot be taken as evidence for the complete absence of any electron flow to
153 NO_3^-. However, the measured NO concentrations lend some support to the claim that V_{eNap} was
154 ~0 until depletion of the externally provided N_2O. In the well-fed culture, the concentration of

155 NO declined to zero in response to depletion of NO_2^-, and increased soon after, as V_{eNap}
156 increased (Figs. 2A and C). Likewise, the NO concentration declined to very low values in
157 response to depletion of NO_2^- in the starved culture (Fig. 2B).

158 Fig. 2C and D show the calculated electron flow rates per cell to the individual reductases,
159 and their sum, illustrating their competition for electrons. This shows that the well-fed cells
160 (Fig. 2C) sustained a nearly constant total electron flow rate around 9 fmol e^- $cell^{-1}$ h^{-1}
161 throughout, but allocated to different reductases depending on the availability of electron
162 acceptors: As long as NO_2^- and N_2O were both present, Nos captured around 50% of the
163 electrons ($V_{eNos} \sim V_{eNir} + V_{eNor}$), increasing to 100% when NO_2^- was depleted after 6-7 hours,
164 while the electron flow rate to Nap remained insignificant until the externally provided N_2O
165 became depleted. The starving cells (Fig. 2D) had an order of magnitude lower total electron
166 flow rate per cell, declining gradually throughout the incubation, and here Nos captured >> 50%
167 of the electrons during the first 10 h ($V_{eNos} >> V_{eNir} + V_{eNor}$), but declined to ~50% towards the
168 end.

169 Bioassay 1 was also used in a second experiment, but in this case the cultures were
170 incubated anoxically ($[O_2]$ <0.21 ±0.04 µM) in buffer containing only one of the N-oxides (NO_3^-,
171 NO_2^- or N_2O) as initial electron acceptor (Figs. 3A-C). This experiment established that starved
172 cultures readily reduced NO_3^- from the start when no other N-oxide was provided (Fig. 3A). It
173 also demonstrated that the cell specific electron flow to N-oxides was practically unaffected by
174 the type of electron acceptor provided, except for the slightly lower rates initially for flasks with
175 NO_2^-. For all treatments, the cell specific electron flow rate decreased gradually throughout,
176 and the levels are very similar to those observed in the first experiment (Fig. 3D).

177

178 **Cell size and PHA accumulation of starved vs well-fed cultures.** The morphologies of single
179 bacterial cells from different treatments (starved/well-fed and anoxic/oxic) were analyzed by
180 phase contrast microscopy (Fig. S1A). By quantifying cell dimensions, we found marginal but
181 statistically significant effects (Mann-Whitney test, $p < 0.01$) of starvation: while there was no
182 significant difference in cell area of individual cells (Fig. S1B), starved cells were on average
183 ~12% longer and ~5% thinner than well-fed cells (Fig. S1B). By further calculating cell volumes, a
184 slight reduction in average cell volume was observed upon starvation of aerobic cells (p=0.057),
185 but not for cells grown under anoxic conditions (Fig. S1C). Furthermore, a qualitative analysis of
186 the presence of PHA granules was done by staining the cells with Nile Red, a lipophilic dye with
187 high affinity for PHA (36). Large foci corresponding to PHA granules were seen in all conditions.
188 It should be noted that, as a lipophilic dye, Nile Red will also bind non-specifically to lipids and
189 membrane, and based on the imaging performed here, it could not be concluded whether there
190 were any significant differences in PHA content between the conditions.

191

192 **Denitrification kinetics after providing starving cultures with an artificial electron donor.**
193 An experiment was then performed in which TMPD plus ascorbate was added to starved
194 cultures (Bioassay 1), to provide cytochrome *c* with an excess of electrons (37,38). Since
195 cultures treated according to Bioassay 1 were able to provide electrons for denitrification (10-
196 18% of the electron flow in well-fed cells during the first 5 h, then decreasing to ca 4%; Fig. 2D),
197 we expected that the TMPD treatment would reduce or eliminate the oxidation of quinol by the
198 *bc1* complex and that this would allow electrons to flow to Nap via NapC, resulting in NO_3^-

199 reduction. We also expected that loading cytochrome *c* with electrons would relieve or weaken
200 the competition for electrons between Nir, Nor and NosZ. The results (Fig. 4) lend little support
201 to the former since the electron flow to Nap remained insignificant until N_2O had been
202 depleted. But the results confirm an effect of TMPD on the competition between Nos and Nir:
203 V_{eNir}, V_{eNor} and V_{eNos} were similar and high (4-5 fmol e^- $cell^{-1}$ h^{-1}) until NO_2^- was depleted. Thus,
204 Nir and Nos competed equally well when the cytochrome *c* pool was fully reduced by TMPD.
205 After depletion of NO_2^-, V_{eNos} leaped to its maximum level, 13-14 fmol N $cell^{-1}$ h^{-1}, and kept this
206 rate until all the exogenous N_2O was depleted.
207
208 **Denitrification kinetics and reductase abundancies of cultures exposed to extended**
209 **starvation following Bioassay 2.** While Bioassay 1 successfully induced starvation in terms of a
210 downshift in respiration, the rates did not reach a stable level during the assay but declined
211 gradually throughout, apparently approaching more stable low levels after 20 h. On this
212 background, we introduced a more severe starvation assay (Bioassay 2, Fig. 1B) by including a
213 20 h aerobic incubation in buffer prior to the starvation-denitrification assay, in order to reach a
214 lower and more stable rate of respiration than in the first experiment. In addition, Bioassay 2
215 was designed to force the cells to synthesize the denitrification proteome while starving. In
216 several preliminary experiments with Bioassay 2 (results not shown), we found a conspicuous
217 variability between flasks regarding the cell specific respiration rate where one or two out of
218 three replicate flasks had four to six times higher cell respiration rates than the other(s). At first,
219 we suspected that it could be due to impurities of flasks or magnets, but meticulous acid
220 washing failed to remove the stochastic variation. Being convinced that the stochasticity

reflects a real regulatory switch of the cultures, we performed a final experiment in which 15 replicate flasks were monitored for denitrification kinetics (Fig. 5).

The cultures received initially 1 mM NO_3^- in the buffer (but no NO_2^-), and He plus 1 ml N_2O (80 µmol N) in headspace. The O_2 concentration at the time of inoculation was <0.5 µM in the liquid. The flasks separated into two distinct denitrification phenotypes (Figs. 5A and B). Nine flasks showed "low" cell specific respiration rates (total electron flow maximum 0.27 fmol e^- $cell^{-1}$ h^{-1}), corresponding to approximately 2.7% compared to well-fed cultures (Fig. 5A), while the other six showed a "fast" respiration rate (total electron flow 1.0-1.8 fmol e^- $cell^{-1}$ h^{-1}). Both phenotypes reduced N_2O from the beginning of the incubation, showing a strong preference for N_2O over NO_3^-. In the flasks with fast respiration, the cells started to reduce NO_3^- in response to depletion of the externally provided N_2O. In the flasks with slow respiration, N_2O was not depleted within the time frame of the experiment, and NO_3^- reduction remained negligible.

To investigate if cell lysis, and thus release of available C, could explain why some cultures showed the "fast" growth phenotype, we compared the OD_{600} and the number of viable cells in "slow" *vs* "fast" cultures. The samples were taken after incubation for 3.1 h in anoxic buffer, when the two phenotypes were clearly distinct but when some possible growth of cells in the "fast" cultures would not yet hide if lysis had occurred. The OD_{600} spanned from 0.12-0.13 with no statistical difference ($p>0.3$) between cultures with "fast" and "slow" respiration. Similarly, no difference ($p=0.4$) was found for the viable counts which showed 1.21E+10 to 1.33E+10 CFU $flask^{-1}$ for the "fast" cultures and 1.23E+10 to 1.34E+10 CFU $flask^{-1}$ for the "slow" cultures (Fig. S2).

We also tested the metabolic integrity of the cells in the flasks with slow respiration by injecting C-substrates (YMB) to the flasks after 24.8 hours, which proved their capacity to quickly regain activity approaching that of well-fed cells (Fig. 5A). To investigate if the observed divergencies in phenotypes were due to differences in denitrification reductase abundancies, we quantified the relative abundances of Nap, NirK and NosZ in samples taken at different time points throughout the incubations (Figs. 5E and F), together with the corresponding denitrification kinetics (Figs. 5A and B) and cell specific electron flow to reductases (Figs. 5C and D). The membrane-bound NO reductase (cNor) could not be extracted quantitatively (the results showed 1000 times lower abundancies than for the other denitrification reductases) and is therefore not shown. The inoculum had been cultured aerobically for 3-4 generations, never permitting the OD_{600} to exceed 0.1, to secure that any denitrification enzymes would be diluted to extinction by aerobic growth, assuming that the transcription of all genes is effectively repressed by oxygen. This strategy was apparently successful since Nap and Nir were undetectable at the start of the anoxic incubation. NosZ, on the other hand, was detected also in the aerobic cultures, suggesting that the *nosZ* gene is constitutively transcribed at low levels in these organisms.

After transferring the cells to anoxic buffer, the abundance of all three reductases increased both in cultures with “slow” and “fast” respiration. Cultures with “slow” respiration rate synthesized less denitrification reductases than those with “fast” respiration rate during the first 20 h. The relative abundances of the different reductases also differed between the two phenotypes. In cultures with “slow” respiration, NosZ was significantly more abundant than Nap and Nir ($p<0.01$), which were comparable (Fig. 5E). Cultures with “fast” respiration instead

contained higher abundancies of NosZ and Nir compared to Nap at 5 h. After this, the abundance of Nir increased more than that of the others and at 20 h the LFQ of Nir was 0.20 ± 0.07, while the abundancies of NosZ and Nap were approximately half of that (Fig. 5F). After addition of carbon substrate to the cultures with "slow" respiration, a rapid synthesis of all three reductases took place. This synthesis was most prominent for Nir which, after a couple of hours, had increased three-fold, reaching a relative abundance that was twice as high as Nap and NosZ (Fig. 5E), resembling the abundance profile of the cultures with "fast" respiration (Fig. 5F).

Discussion

Detailed eco-physiological studies during the past decades have revealed several aspects of how the denitrification process is regulated in different organisms (6,13,39). Most of this knowledge is, however, based on laboratory studies where cultures have been grown under optimal conditions, while less attention has been paid to understanding how denitrification, and particularly the release of N_2O, is affected if cells are starved, which is the normal state of cells in most natural environments. We focused on how starvation, i. e. lack of carbon substrate, affects denitrification and N_2O release. The general notion has been that N_2O reductase is less competitive for electrons than the other denitrification reductases, leading to emissions of N_2O when the availability of electron donors is low. This is largely based on a single study of *Alcaligenes faecalis* (40) and has been supported by some studies of complex communities but contested by others (41-43). *A. faecalis* can perform partial denitrification reducing NO_2^- to N_2 using NirK, cNor and NosZ clade I, but this organism lacks dissimilatory NO_3^- reductases (Nar or

Nap). The study by Schalk-Otto (40), performed in continuous cultures, showed increased N_2O release under low substrate concentrations, and it was suggested that N_2O reductase did not compete successfully with the other reductases for electrons from cytochrome *c*, possibly due to lower affinity for the electron donor. This conclusion needs, however, further verification by more detailed studies of the mechanism involved. Moreover, such studies need to be extended to other groups of denitrifying microorganisms and should include organisms carrying a complete denitrification pathway (thus with Nar and/or Nap). Research over the past decades has revealed diverse denitrification phenotypes among even closely related bacteria, with implications for their accumulation of denitrification intermediate products (15,44).

The phenotype described for a range of taxonomically diverse *Bradyrhizobium* strains with a complete denitrification pathway is characterized by a strong preference for N_2O over NO_3^- when grown in full-strength YMB medium under denitrifying conditions (18,19). The present study provides compelling evidence that this preference is retained when the organisms are starved for carbon and energy, with practically no electron flow to Nap when N_2O was present (Figs. 2A-D). This was not due to too low levels of Nap since the cultures showed well-functioning Nap activity if NO_3^- was provided as the only initial electron acceptor (Fig. 3A). Further evidence for this was obtained from the proteomics results, which showed that the cultures, even when grown under more severe starvation conditions using Bioassay 2, were able to produce comparable amounts of Nap, Nir and Nos (Figs. 5E and F). Therefore, the lack of NO_3^- reduction during the period when there was N_2O in the system could not be explained by a lack of Nap molecules. Instead, the results suggest the same metabolic-level phenomenon as

found for well-fed cultures in this study (Fig. 2A) and earlier (18,19), where NosZ outcompetes Nap for electrons, leaving Nap virtually without electrons so long as exogenous N_2O is available.

The attempt to tweak the electron flow toward Nap by the addition of TMPD and ascorbate did not result in measurable NO_3^- reduction in the starved cultures (Fig. 4A). A recent study by Mania et al. (18) demonstrated that well-fed *Bradyrhizobium* cells did reduce some NO_3^- in the presence of N_2O, if provided with TMPD and ascorbate. This suggested that NosZ (as well as Nir and Nor) received electrons from strongly reduced cytochrome *c*, thus bypassing the electron flow via the *bc1* complex, which allowed Nap to receive electrons from quinol, delivered from the TCA cycle. The specificity of the electron delivery from TMPD to cytochrome *c* cannot be taken for granted, however, and the result by Mania et al. (18) could instead reflect a minimum of electron flow from TPMD to quinon or to NapC, directly, or indirectly. In the present experiment with starved cells, TMPD + ascorbate failed to induce measurable electron flow to Nap in the presence of N_2O (Fig. 4B). This probably reflects the marginal electron flow from the TCA cycle to the quinon/quinol pool due to starvation. A separate experiment supported this, showing that when carbon substrate (YMB) was added to starved cultures, this provided enough electrons to support some Nap activity, although NosZ activity still dominated (Fig. S3).

At the same time, the result refutes the concerns regarding unspecific electron delivery of electrons from TMPD to quinon. Functional Nap was apparently present, and NO_3^- reduction started when N_2O was almost depleted, with V_{eNap} being 2 fmol e^- $cell^{-1}$ h^{-1} which was twice as high as $V_{eNir/Nor}$ (Fig. 4B). The latter is as expected, since the reduction of 1 mole of NO_3^- to NO_2^- requires 2 mole electrons, while reduction of NO_2^- and NO requires 1 mole electrons. Furthermore, the electron flow to NosZ was the same as to Nir and Nor, suggesting that Nir and

NosZ competed equally well for electrons from cytochrome *c*. The maximum total electron flow of 13-14 fmol e^- $cell^{-1}$ h^{-1} when the cytochrome *c* pool was saturated with electrons from TMPD is likely to be close to the maximum capacity of the denitrification pathway. This electron flow rate is higher than the total electron flow rate in the well-fed cells, which was 8-10 fmol e^- $cell^{-1}$ h^{-1} (Fig. 2C). The factor limiting V_{eNos} to 13-14 fmol $cell^{-1}$ h^{-1} is plausibly the rate of electron delivery from cytochrome *c* and/or k_{cat} for Nos.

In another experiment we added YMB medium to "slow respiration" phenotypes of the cultures that had been exposed to extended starvation (Figs. 5A, C and E). These cultures had some NosZ activity (V_{eNos} 0.1-0.3 fmol e^- $cell^{-1}$ h^{-1}), while Nap and Nir activities could not be detected. Addition of the electron donor (YMB) led to an immediate upshoot in the activities of all reductases. This could not have been the case if the reductases were not present already, which was proven by the proteomics results. Taken together, the results support that the absolute preference for N_2O over NO_3^- was due to competition for electrons, also under severe starvation conditions.

It is well known that bacteria have developed a range of physiological responses to tackle starvation. Some survive by forming spores, but most bacteria survive by strongly reduced metabolic rates and minimizing the synthesis of some proteins while upregulating others such as genes for high-affinity transporters, essential repair mechanisms and alternative energy sources (3,45,46). Some such changes have been observed in rhizobia belonging to *Rhizobium leguminosarum*, which stayed viable for long periods (55 days) of C starvation (47). Changes in cell size are common during long-term starvation, sometimes leading to the formation of small or even ultra-microcells which may have increased tolerance to antibiotics and other stresses

(2,46). Another way for many bacteria, including rhizobia, to survive is to use carbon stored as polyhydroxyalkanoates (PHA) or glycogen, formed during periods of ample nutrient abundance (48). In the present study, the metabolic activity, measured as anaerobic respiration rate, decreased to between 1 and 18% that of well-fed cultures, depending on which starvation bioassay was used. We did not, however, detect any obvious decrease in cell size when comparing cells starved for 24 h, although cell morphologies were slightly altered (Figs. S1A and B). PHA was observed in the starved cells as well as well-fed ones, as shown with Nile red staining (Fig. S1A) and no obvious reduction in PHA could be observed during starvation from our assays. Since this was a comparably short period of starvation, it is conceivable that the cells would make use of the stored carbon if the starvation was prolonged. It could be speculated that one reason for not using the PHA reserves (and glycogen) immediately, is that these are saved to be used during bacteroid formation (48). To clarify these issues, more detailed studies are however needed.

A striking separation into two phenotypes during starvation, as shown in Fig. 5, was observed in repeated experiments (Bioassay 2), each time with about two thirds of the flasks showing a "fast" and the others "slow" respiration: 1.0-1.8 fmol e^- $cell^{-1}$ h^{-1} vs 0.1-0.3 fmol e^- $cell^{-1}$ h^{-1}, respectively. Phenotypic heterogeneity has been observed in single-strain cultures of various bacteria when exposed to carbon substrate deficiency and may, or may not, be due to mutations during starvation for one week or more (3,49). Mutations in the entire population in several replicate flasks are unlikely and cannot, however, have caused the rapid diversification into "slow"- or "fast" respiration in the present study. It may instead reflect a stochastic phenomenon, or that the culture contained different subpopulations. We speculated that the

373 "fast respiration" phenotype may be due to a fraction of the cells dying, allowing the other cells
374 to survive on nutrients released from lysed cells, as seen for other bacteria (3). However, this
375 would require lysis of a substantial fraction of the cells, which is refuted by the observation that
376 the flasks with "slow" and "fast" phenotypes had practically identical numbers of viable cells
377 (Fig. S2). Thus, further studies are needed to understand this phenomenon of different
378 respiration rates.

379 Although the starvation bioassays developed for this study cannot be regarded as a close
380 mimicking of the conditions in natural environments, it is conceivable from the experiments
381 that these organisms are potentially strong sinks for N_2O when living in soil under fluctuating
382 availability of carbon substrate. Bioassay 1 is probably closer to a "real-world" situation than
383 Bioassay 2, since it is likely that denitrifying bacteria experience regular fluctuations in oxygen
384 and thus are not devoid of denitrification reductases if they enter starvation. On the other hand,
385 Bioassay 2, where the cells had to produce the denitrification proteome in the absence of
386 external electron donors (C-substrate), showed that even under these conditions N_2O reduction
387 strongly dominated over NO_3^- reduction.

388

389 **Materials and methods**

390 **Bacterial strain and culture preparations.** *Bradyrhizobium* strain HAMBI 2125, originally
391 isolated from nodules of *Arachis hypogaea* growing in Sichuan, China (50), was used in all
392 experiments. This strain, which is closely related to *Bradyrhizobium ottawaense*, contains the
393 genetic set-up for complete denitrification (19). A culture was raised from one single colony
394 after streaking on agar plates. After checking the purity by sequencing the 16S rRNA gene (19),

395 portions were preserved in 15% glycerol at -80 °C. Cultures for all the experiments were started
396 from the -80 °C stocks and raised under fully oxic conditions in 120 ml serum flasks containing
397 50 ml Yeast Mannitol Broth (YMB): 10 g l^{-1} D-Mannitol, 0.5 g l^{-1} K_2HPO_4, 0.2 g l^{-1} $MgSO_4 \cdot 7H_2O$,
398 0.1 g l^{-1} NaCl and 0.5 g l^{-1} yeast extract (51). All incubations were done at 28 °C. Medical flasks
399 (120 ml) were used in all experiments. A magnet in each flask secured vigorous stirring (600-
400 700 rpm) to avoid cell aggregation and to optimize the gas exchange between liquid and gas
401 phases (18). To prevent that the cells experienced anoxia during this oxic incubation, and thus
402 to avoid de novo synthesis of denitrification reductases, portions were regularly transferred to
403 new flasks containing fresh medium, so that the OD_{600} was never allowed to exceed 0.1 (19).
404 These aerobically grown cultures were used as inoculants in the "starvation bioassays"
405 described below.

406 Flasks for cultures incubated under hypoxic conditions were prepared as described in (18).
407 Briefly, flasks (120 ml) containing 50 ml buffer (or medium) were capped with sterilized, gas
408 tight butyl rubber septa (Matrix AS, Norway). The air was removed by applying vacuum
409 repeatedly (6 x 360 s) and He was then filled for 30 s, after which the overpressure was
410 released. The flasks were left for two days to equilibrate the gases between the headspace and
411 liquid (52). Then, 0.7 ml or 1 ml O_2 (equal to 1 or 1.5 vol %) and 1 ml N_2O (70 to ~80 µmol N
412 $flask^{-1}$) was injected into the headspace and sterile filtered solutions of KNO_3 (and sometimes
413 KNO_2) were added to the liquid reaching initial, desired concentrations (0.25 -1 mM).

414

415 **Starvation bioassays.** Starvation bioassays were established, which followed one of the
416 procedures described in Fig. 1. In Bioassay 1 "Mild starvation", cultures were allowed to make

the transition to denitrification in full-strength YMB before being exposed to starvation. Oxically grown, well-fed cultures were incubated for 48 h after which the headspace was replaced by He and 1% O_2, and 1 mM KNO_3 was added to the medium. When O_2 was depleted, the cultures were centrifuged (10 000 × g at 4 °C for 10 min) and washed twice in sterile ddH_2O. The pellets (triplicates) were pooled to reduce bias in the form of variations due to the centrifugation/washing. Each pellet was divided into three and used to inoculate anoxic flasks containing 50 ml C-free buffer supplemented with 1 mM KNO_3 and 0.25 or 0.5 mM KNO_2 and with He and/or 1 ml N_2O (around 80 µmol N $flask^{-1}$) in the headspace. When incubated in the buffer, the respiration rate of the cultures was 10-18% that of well-fed cultures during the first 15 h, then it decreased to about 4%.

In Bioassay 2 ("extended starvation"), denitrification was instead induced after having exposed the cells to starvation for 20 h. The cultures were raised in fully oxic flasks containing YMB medium. When OD_{600} reached ~0.1, the cultures were centrifuged (10 000 × g at 4 °C for 10 mins) and washed twice in sterile ddH_2O. The pellets (triplicates) were pooled after which they were evenly divided and used to inoculate fully oxic flask containing C-free "starvation buffer". These cultures were incubated for 20 h, then centrifuged after which the pellets were pooled and divided evenly before being inoculated into flasks containing C-free "starvation buffer" with 1 mM KNO_3, and with He and 1 ml N_2O (around 80 µmol N $flask^{-1}$) in headspace. The respiration rate of cultures exposed to "extended starvation" was ca 1-4% compared to that of well-fed cultures. Results from the different starvation bioassays were compared to those from well-fed cultures. To avoid biases, the treatments, which were in all cases set up at least in triplicates ($n \geq 3$), were the same regarding centrifugations and washings until the last

439 step when pooled cells were inoculated to anoxic flasks containing either YMB or buffer. The
440 carbon source in the YMB medium comprised >200 times surplus of electron donor compared
441 to electron acceptors throughout all incubations, thus ensuring that the electron donor was not
442 depleted. All cultures were incubated at 28°C, and with vigorous stirring (600-700 rpm).
443
444 **Addition of YMB medium or TMPD as electron donors to starved cultures.** Experiments
445 were performed to investigate how starved cultures of *Bradyrhizobium* strain HAMBI 2125
446 responded to the addition of an electron donor, either provided as an artificial electron donor
447 (Fig. 4) or as YMB medium (2 ml mannitol /yeast solution providing them with a substrate
448 concentration corresponding to half-strength YMB, thus 5 g mannitol and 0.25 g yeast l^{-1}, Fig. 5).
449 As artificial electron donor we used sodium TMPD (N, N, N´, N´-tetramethyl-p-
450 phenylenediamine) which, in the presence of ascorbate, donates electrons to cytochrome c
451 thus providing electrons to Nir and NosZ (18,37). Ascorbate and TMPD (both from Sigma-
452 Aldrich®, Germany) were dissolved in ddH_2O or 96% ethanol, respectively, and filter sterilized.
453 The solutions were added to the incubation flasks 10-15 mins before gas sampling. The effect of
454 different concentrations of TMPD (100, 250, and 500 µM in the culture buffer) combined with
455 10 mM ascorbate on N_2O reduction was checked prior to the main experiments. This showed
456 that 500 µM TMPD had an obvious inhibition effect on N_2O reduction, while 100 µM and 250
457 µM showed no inhibitory effect (not shown). To minimize other, possible effects we used 100
458 µM TMPD for the experiments (as done in Mania et al. (18)). In another experiment, shown in
459 Fig. S3, 4 ml of a mannitol/yeast solution was added to flasks containing 50 ml starved cultures,

460 providing them with a substrate concentration corresponding to full strength YMB (10 g
461 mannitol and 0.5 g yeast l^{-1}).
462
463 **Monitoring of gas kinetics, NO_3^- and NO_2^- concentrations and electron flow rates.** The
464 culture flasks were placed in a robotized incubation system and the headspace gas was sampled
465 frequently for N_2, N_2O, NO and O_2 measurements (34). Gas losses caused by sampling were
466 taken into account when calculating the production and consumption of gases, as described by
467 Molstad et al. (34) and Mania et al. (18). The concentration of O_2 in the anoxic incubation flasks
468 was <0.6 µM at the start of the experiment, which was well below the level for initiating
469 denitrification (4.6 µM; (19)).
470 The NO_2^- concentrations were monitored as described in Mania et al. (18). Briefly, samples
471 (0.1- 0.5 ml) were taken every 1 or 2 hours (n=3) from the liquid phase through the septum of
472 the flasks using a sterile syringe. To avoid that the gas kinetics was affected by the sampling, a
473 set of flasks was dedicated to NO_2^- measurements and a parallel set was left untouched for gas
474 measurements. NO_2^- was determined using a chemoluminescence NOx analyzer (Sievers NOA^{TM}
475 280i, GE Analytical Instruments) after at first reducing the NO_2^- to NO by adding 10 µl liquid
476 sample into a purging device containing a reducing agent (50% acetic acid with 1% (w/v) NaI)
477 (53,54). The NO_2^- concentrations were determined against a standard curve (range 0-2 mM
478 NO_2^-; r^2= 0.999).
479 The cell specific electron flow rates (V_e, mol e^- $cell^{-1}$ h^{-1}) for each time increment between
480 two gas samplings were calculated as $V_{eflask}(t)/(N(0)+E_{cum}(t)*Y)$, where $V_{eflask}(t)$ is the electron
481 flow rate in the flask (mol e^- $flask^{-1}$ h^{-1}) calculated from measurements, $N(0)$ is number of cells in

482 the flask at time=0, $E_{cum}(t)$ is the cumulated electron flow (mol e^- $flask^{-1}$) at time=t , and Y is the
483 yield per mol electron (cells mol^{-1} e^-) for HAMBI 2125 as measured previously (19). The
484 conversion factor 5.8E8 cells ml^{-1} *OD_{600}^{-1} was used to convert OD_{600} to cell numbers (19).
485
486 **Proteomics**. The abundances of Nap, Nir and NosZ were quantified in starved cultures
487 treated as described for Bioassay 2 (extended starvation). Altogether eighteen flasks were
488 prepared according to Fig. 1B. After the 20 h aerobic incubation in C-free buffer, three flasks
489 were harvested for proteomics analysis and, following centrifugation/washing, the three cell
490 pellets from these flasks were frozen individually at -20 °C. The cultures in the other flasks were
491 pooled three by three and after centrifugation/washing, each cell pellet was divided in three
492 and used to inoculate new flasks containing C-free buffer with NO_3^- in the liquid and with He
493 and 1 ml N_2O in the headspace (Fig. 1B). These flasks (fifteen in total) were placed in the robotic
494 incubation system for monitoring of gas kinetics and NO_2^- concentrations as described above.
495 The entire culture volume (50 ml) was harvested from each of triplicate flasks at different time
496 points during the anoxic incubation. The cultures in six of the flasks showed a “fast” respiration
497 rate (total electron flow 1.0-1.8 e^- $cell^{-1}$ h^{-1}) and were harvested at 5 and 20 h of incubation in
498 anoxic buffer (triplicates at each sampling point). The cultures in the other nine flasks showed a
499 “slow” respiration rate (maximum total electron flow rate was 0.27 fmol e^- $cell^{-1}$ h^{-1}). Six of
500 them were harvested in triplicates after 10 and 20 h in anoxic buffer. The remaining three flasks
501 from the cultures with “slow” respiration rate received a portion of YMB at 24.8 hand were
502 harvested at 27 h. Harvested cell cultures were centrifuged and stored as pellets at -20 °C. The
503 protein extraction was as described in Gao et al. (19). Briefly, the thawed cell pellets were

resuspended in lysis buffer (20 mM Tris–HCl pH 8, 0.1% v/v Triton X-100, 200 mM NaCl, 1 mM DTT). They were then subjected to bead beating (3 × 45 s) with glass beads (particle size ≤ 106 µm; Sigma) using a MP Biomedicals™ FastPrep-24™ (Thermo Fischer Scientific) at maximum power and with cooling on ice between the cycles. After centrifugation to remove cell debris (10 000 × g; 5 min), the supernatant, containing water soluble proteins, was used for proteomic analysis using an Orbitrap mass spectrometer (described in (19,55)). Quantification was based on LFQ (label-free quantification) in MaxQuant (56), and the relative abundance of the individual reductases was calculated as percentages of the sum of all protein abundances for each time point. The nitric oxide reductases NorB/C were not measured since only a small fraction of these membrane-bound enzymes can be accurately obtained with this extraction protocol (approximately 1/1000th the quantity of the other reductases).

Viable counts and microscopy. The number of viable cells in starved cultures showing slow and fast respiration rates, observed in flasks prepared according to Bioassay 2, was determined by plating dilutions of the cultures on yeast-mannitol agar (YMA). The morphology of cells from well-fed cultures and starved cultures was compared using phase contrast microscopy and a qualitative determination (presence/absence) of PHA was done by staining with Nile Red (Sigma-Aldrich) followed by fluorescence microscopy. Microscopy was performed on a Zeiss AxioObserver with an Orca-Flash4.0 CMOS camera (Hamamatsu Photonics) controlled by the ZEN Blue software. Images were taken with a 100x phase contrast objective. A HPX-120 Illuminator was used as light source for fluorescence microscopy. Images were prepared using ImageJ and analysis of cell sizes was done using the ImageJ-plugin MicrobeJ (57).

Acknowledgment

This project was supported by Kingenta Ecological Engineering Group Co., LTD and by the project PASUSI financed by the EC Horizon2020 ERA-NET Cofund Programme, Grant agreement No. 727715 and by the Research Council of Norway, projects No. 290488 and 325770. Yuan Gao is grateful to the China Scholarship Council (CSC) for financial support. We thank Gro Stamsås for help with microscopy.

References

1. Hobbie JE, Hobbie EA. 2013. Microbes in nature are limited by carbon and energy: The starving-survival lifestyle in soil and consequences for estimating microbial rates. Front Microbiol 4:324.
2. Morita RY. 1990. The starvation-survival state of microorganisms in nature and its relationship to the bioavailable energy. Experientia 46:813–817.
3. Bergkessel M, Basta DW, Newman DK. 2016. The physiology of growth arrest: Uniting molecular and environmental microbiology. Nat Rev Microbiol 14:549–562.
4. Ratcliff WC, Kadam SV, and Denison, R.F. 2008. Poly-3-hydroxybutyrate (PHB) supports survival and reproduction in starving rhizobia. FEMS Microbiol Ecol 65:391–399.
5. Müller-Santos M, Koskimäki JJ, Alves LPS, de Souza EM, Jendrossek D, Pirttilä AM. 2021. The protective role of PHB and its degradation products against stress situations in bacteria. FEMS Microbiol Rev 45:fuaa058.

6. Zumft WG. 1997. Cell biology and molecular basis of denitrification. Microbiol Mol Biol Rev 61:533–616.
7. Duffner C, Kublik S, Fösel B, Frostegård Å, Schloter M, Bakken L, Schulz S. 2022. Genotypic and phenotypic characterization of hydrogenotrophic denitrifiers. Environ Microbiol 24:1887-1901.
8. Schneider LK, Wüst A, Pomowski A, Zhang L, Einsle O. 2014. No laughing matter: The unmaking of the greenhouse gas dinitrogen monoxide by nitrous oxide reductase. Met Ions Life Sci 14:177–210.
9. Hein S, Simon J. 2019. Bacterial nitrous oxide respiration: electron transport chains and copper transfer reactions. Adv Microb Physiol 75:137–175.
10. Shapleigh JP. 2013. Denitrifying prokaryotes: Prokaryotic Physiology and Biochemistry. In Rosenberg E, DeLong EF, Lory S, Stackebrandt E, Thompson F. (eds), The prokaryotes, pp. 405-425. Berlin, Heidelberg: Springer.
11. Graf DRH, Jones CM, Hallin S. 2014. Intergenomic comparisons highlight modularity of the denitrification pathway and underpin the importance of community structure for N_2O emissions. PLoS ONE 9:e114118.
12. Richardson D, Felgate H, Watmough N, Thomson A, Baggs E. 2009. Mitigating release of the potent greenhouse gas N_2O from the nitrogen cycle - could enzymic regulation hold the key? Trends Biotechnol 27:388-97.
13. Spiro S. 2012. Nitrous oxide production and consumption: regulation of gene expression by gas-sensitive transcription factors. Philos Trans R Soc Lond B Biol Sci 367:1213-25.

14. Liu B, Frostegård Å, Bakken LR. 2014. Impaired reduction of N_2O to N_2 in acid soils is due to a posttranscriptional interference with the expression of *nosZ*. mBio 5:e01383-14.

15. Liu B, Mao Y, Bergaust L, Bakken LR, Frostegård A. 2013. Strains in the genus *Thauera* exhibit remarkably different denitrification regulatory phenotypes. Environ Microbiol 15:2816-28.

16. Gaimster H, Alston M, Richardson DJ, Gates AJ, Rowley G. 2018. Transcriptional and environmental control of bacterial denitrification and N_2O emissions. FEMS Microbiol Lett 365:fnx277.

17. Lycus P, Soriano-Laguna MJ, Kjos M, Richardson DJ, Gates AJ, Milligan DA, Frostegård Å, Bergaust L, Bakken LR. 2018. A bet-hedging strategy for denitrifying bacteria curtails their release of N_2O. Proc Natl Acad Sci 115:11820–11825.

18. Mania D, Woliy K, Degefu T, Frostegård Å. 2020. A common mechanism for efficient N_2O reduction in diverse isolates of nodule-forming bradyrhizobia. Environ Microbiol 22:17–31.

19. Gao Y, Mania D, Mousavi SA, Lycus P, Arntzen M, Woliy K, Lindström K, Shapleigh JP, Bakken LR, Frostegård Å. 2021. Competition for electrons favours N_2O reduction in denitrifying *Bradyrhizobium* isolates. Environ Microbiol 23:2244–2259.

20. Butterbach-Bahl K, Baggs EM, Dannenmann M, Kiese R, Zechmeister-Boltenstern S. 2013. Nitrous oxide emissions from soils: How well do we understand the processes and their controls? Philos Trans R Soc Lond B Biol Sci 368:20130122.

21. Thompson RL, Lassaletta L, Patra PK, Wilson C, Wells KC, Gressent A, Koffi EN, Chipperfield M, Winiwarter W, Davidson EA, Tian H, Canadell JG. 2019. Acceleration of global N_2O emissions seen from two decades of atmospheric inversion. Nat Clim Change 9:993–998.

590 22. Tian H, Lu C, Ciais P, Michalak AM, Canadell JG, Saikawa E, Huntzinger DN, Gurney KR, Sitch
591 S, Zhang B, Yang J, Bousquet P, Bruhwiler L, Chen G, Dlugokencky E, Friedlingstein P, Melillo
592 J, Pan S, Poulter B, Prinn R, Saunois M, Schwalm CR, Wofsy SC. 2016. The terrestrial
593 biosphere as a net source of greenhouse gases to the atmosphere. Nature 531:225–228.
594 23. Tian H, Xu R, Canadell JG, Thompson RL, Winiwarter W, Suntharalingam P, Davidson EA,
595 Ciais P, Jackson RB, Janssens-Maenhout G, Prather MJ, Regnier P, Pan N, Pan S, Peters GP,
596 Shi H, Tubiello FN, Zaehle S, Zhou F, Arneth A, Battaglia G, Berthet S, Bopp L,
597 Bouwman AF, Buitenhuis ET, Chang J, Chipperfield MP, Dangal, SRS, Dlugokencky E,
598 Elkins JW, Eyre BD, Fu B, Hall B, Ito A, Joos F, Krummel PB, Landolfi A, Laruelle GG,
599 Lauerwald R, Li W, Lienert S, Maavara T, MacLeod M, Millet DB, Olin S, Patra PK, Prinn RG,
600 Raymond PA, Ruiz DJ, van der Werf GR, Vuichard N, Wang J, Weiss RF, Wells KC, Wilson
601 C, Yang J, Yao Y. 2020. A comprehensive quantification of global nitrous oxide sources and
602 sinks. Nature 586: 248–256.
603 24. Davidson EA, Kanter D. 2014. Inventories and scenarios of nitrous oxide emissions. Environ
604 Res Lett 9:105012.
605 25. Bakken LR, Frostegård Å. 2020. Emerging options for mitigating N_2O emissions from food
606 production by manipulating the soil microbiota. Curr Opin Environ Sustain 47:89–94.
607 26. Jensen ES, Peoples MB, Boddey RM, Gresshoff PM, Henrik HN, Alves BJR, Morrison MJ. 2012.
608 Legumes for mitigation of climate change and the provision of feedstock for biofuels and
609 biorefineries. A review. Agron Sustain Dev 32:329-364.
610 27. Poole P, Ramachandran V, Terpolilli J. 2018. Rhizobia: From saprophytes to endosymbionts.
611 Nat Rev Microbiol 16:291–303.

612 28. Hénault C, Revellin C. 2011. Inoculants of leguminous crops for mitigating soil emissions of
613 the greenhouse gas nitrous oxide. Plant Soil 346:289–296.
614 29. Itakura M, Uchida Y, Akiyama H, Hoshino YT, Shimomura Y, Morimoto S, Tago K, Wang Y,
615 Hayakawa C, Uetake Y, Sánchez C, Eda S, Hayatsu M, Minamisawa K. 2013. Mitigation of
616 nitrous oxide emissions from soils by *Bradyrhizobium japonicum* inoculation. Nat Clim
617 Change 3:208–212.
618 30. Jaiswal SK, Dakora FD. 2019. Widespread distribution of highly adapted *Bradyrhizobium*
619 species nodulating diverse legumes in Africa. Front Microbiol 10:310.
620 31. Woliy K, Degefu T, Frostegård Å. 2019. Host Range and Symbiotic Effectiveness of N_2O
621 Reducing Bradyrhizobium Strains. Front Microbiol 10:2746.
622 32. Bedmar EJ, Robles EF, Delgado MJ. 2005. The complete denitrification pathway of the
623 symbiotic, nitrogen-fixing bacterium *Bradyrhizobium japonicum*. Biochem Soc Trans 33:141-
624 144.
625 33. Narozna D, Pudełko K, Króliczak J, Golińska B, Sugawara M, Mądrzak CJ, Sadowsky MJ. 2015.
626 Survival and competitiveness of *Bradyrhizobium japonicum* strains 20 years after
627 introduction into field locations in Poland. Appl Environ Microbiol 81:5552–5559.
628 34. Molstad L, Dörsch P, Bakken LR. 2007. Robotized incubation system for monitoring gases
629 (O_2, NO, N_2O, N_2) in denitrifying cultures. J Microbiol Methods 71:202–211.
630 35. Lim NYN, Frostegård Å, Bakken LR. 2018. Nitrite kinetics during anoxia: The role of abiotic
631 reactions versus microbial reduction. Soil Biol Biochem 119:203–209.
632 36. Spiekermann P, Rehm BH, Kalscheuer R, Baumeister D, Steinbüchel A. 1999. A sensitive,
633 viable-colony staining method using Nile red for direct screening of bacteria that

634 accumulate polyhydroxyalkanoic acids and other lipid storage compounds. Arch Microbiol
635 171:73-80.
636 37. Kimelberg HK, Nicholls P. 1969. Kinetic studies on the interaction of TMPD with cytochrome
637 *c* and cytochrome *c* oxidase. Arch Biochem Biophys 133:327–335.
638 38. Bueno E, Richardson DJ, Bedmar EJ, Delgado MJ. 2009. Expression of *Bradyrhizobium*
639 *japonicum* cbb3 terminal oxidase under denitrifying conditions is subjected to redox control.
640 FEMS Microbiol Lett 298:20–28.
641 39. Torres MJ, Simon J, Rowley G, Bedmar EJ, Richardson DJ, Gates AJ, Delgado MJ. 2016.
642 Nitrous Oxide Metabolism in Nitrate-Reducing Bacteria: Physiology and Regulatory
643 Mechanisms. Adv Microb Physiol 68:353-432.
644 40. Schalk-Otte S, Seviour R, Kuenen J, Jetten MSM. 2000. Nitrous oxide (N_2O) production by
645 *Alcaligenes faecalis* during feast and famine regimes. Water Res 34:2080-2088.
646 41. Itokawa H, Hanaki K, Matsuo T. 2001. Nitrous oxide production in high-loading biological
647 nitrogen removal process under low COD/N ratio condition. Water Res 35:657-664.
648 42. Lu H, Chandran K. 2010. Factors promoting emissions of nitrous oxide and nitric oxide from
649 denitrifying sequencing batch reactors operated with methanol and ethanol as electron
650 donors. Biotechnol Bioeng 106:390-8.
651 43. Pan Y, Ni BJ, Bond PL, Ye L, Yuan Z. 2013. Electron competition among nitrogen oxides
652 reduction during methanol-utilizing denitrification in wastewater treatment. Water Res
653 47:3273-81.

654 44. Lycus P, Bøthun KL, Bergaust L, Shapleigh JP, Bakken LR, Frostegård Å. 2017. Phenotypic and
655 genotypic richness of denitrifiers revealed by a novel isolation strategy. ISME J 11:2219–
656 2232.
657 45. Kjelleberg S, Albertson N, Flärdh K, Holmquist L, Jouper-Jaan A, Marouga R, Ostling J,
658 Svenblad B, Weichart D. 1993. How do non-differentiating bacteria adapt to starvation?
659 Antonie Van Leeuwenhoek 63:333-41.
660 46. Gray DA, Dugar G, Gamba P, Strahl H, Jonker MJ, Hamoen LW. 2019. Extreme slow growth
661 as alternative strategy to survive deep starvation in bacteria. Nat Commun 10:890.
662 47. Thorne SH, Williams HD. 1997. Adaptation to nutrient starvation in Rhizobium
663 leguminosarum bv. phaseoli: analysis of survival, stress resistance, and changes in
664 macromolecular synthesis during entry to and exit from stationary phase. J Bacteriol
665 179:6894-901.
666 48. Lodwig EM, Leonard M, Marroqui S, Wheeler TR, Findlay K, Downie JA, Poole PS. 2005. Role
667 of polyhydroxybutyrate and glycogen as carbon storage compounds in pea and bean
668 bacteroids. Mol Plant Microbe Interact 18:67-74.
669 49. Chen H, Chen CY. 2014. Starvation induces phenotypic diversification and convergent
670 evolution in *Vibrio vulnificus*. PLoS One 9:e88658.
671 50. Zhang X, Nicki G, Kaijalaineni S, Terefework Z, Paulin L, Tighe SW, Graham PH, Lindström K.
672 (1999) Phylogeny and Diversity of *Bradyrhizobium* Strains Isolated from the Root Nodules of
673 Peanut (Arachis hypogaea) in Sichuan, China. Syst Appl Microbiol 22:378-386.
674 51. Schwartz W. 1972. Vincent, J.M. A Manual for the Practical Study of the Root-Nodule
675 Bacteria (IBP Handbuch No. 15 des International Biology Program, London). XI u. 164 S., 10

676 Abb., 17 Tab., 7 Taf. Oxford-Edinburgh 1970: Blackwell Scientific Publ., 45 s. Z Allg Mikrobiol
677 12:1521-4028.
678 52. Mania D, Heylen K, van Spanning RJ, Frostegård Å. 2016. Regulation of nitrogen metabolism
679 in the nitrate-ammonifying soil bacterium *Bacillus vireti* and evidence for its ability to grow
680 using N_2O as electron acceptor. Environ Microbiol 18:2937-50.
681 53. Cox RD. 1980. Determination of nitrate and nitrite at the parts per billion level by
682 chemiluminescence. Anal Chem 52:332–335.
683 54. MacArthur PH, Shiva S, Gladwin MT. 2007. Measurement of circulating nitrite and S-
684 nitrosothiols by reductive chemiluminescence. J Chromatogr B Analyt Technol Biomed Life
685 Sci 851:93–105.
686 55. Conthe M, Lycus P, Arntzen MØ, Ramos da Silva A, Frostegård Å, Bakken LR, Kleerebezm R,
687 van Loosdrecht MCM. 2019. Denitrification as an N_2O sink. Water Res 151:381–387.
688 56. Cox J, Mann M. 2008. MaxQuant enables high peptide identification rates, individualized
689 p.p.b.-range mass accuracies and proteome-wide protein quantification. Nat Biotechnol
690 26:1367-72.
691 57. Ducret A, Quardokus EM, Brun YV. 2016. MicrobeJ, a tool for high throughput bacterial cell
692 detection and quantitative analysis. Nat Microbiol 20:16077.

693

694 **Figure legends**

695 **FIG 1** Bioassays for assessing the effect of starvation on electron flow to denitrification enzymes.
696 A: Bioassay 1: starvation of cells with a previously expressed denitrification proteome. Cells
697 were raised from stock cultures in fully oxic flasks containing YMB medium. When OD_{600}

reached ~0.1, the flasks were made anoxic by He-washing, then supplemented with 1% O_2 in the headspace and 1 mM NO_3^- in the liquid. The cultures were allowed to deplete the O_2 and to initiate denitrification when growing in YMB medium, after which they were centrifuged (10 000 × g at 4 °C for 10 mins) and washed twice in sterile ddH_2O. The pellets from triplicate flasks were pooled and used to inoculate flasks containing either C-free buffer or YMB medium (well-fed control), in both cases supplemented with 1 mM KNO_3 and 0.25 or 0.5 mM KNO_2, and with He and 1 ml N_2O (around 80 µmol N $flask^{-1}$) in headspace. The starving cells, incubated in buffer, had a low respiratory electron flow rate (mol electrons $cell^{-1}$ h^{-1}), initially being 10-18 % that of the well-fed cultures, and then decreasing to reach around 4% after 20 h. Results from experiments using Bioassay 1 are presented in Figs. 2, 3 and 4.

B: Bioassay 2: denitrification induced during starvation. Cells were raised from stock cultures in fully oxic flasks containing YMB medium. When OD_{600} reached ~0.1, the cultures were centrifuged (10 000 × g at 4 °C for 10 mins) and washed twice in sterile ddH_2O. The pellets from triplicate flasks were pooled, after which they were evenly divided and used to inoculate fully oxic flasks containing C-free buffer. These cultures were incubated for 20 h, then centrifuged after which the pellets were pooled and divided evenly before being inoculated into flasks containing C-free buffer-provided with 1 mM KNO_3, and with He and 1 ml N_2O (around 80 µmol N $flask^{-1}$) in headspace. The respiration rate (mol electrons $cell^{-1}$ h^{-1}) of the starving cultures was 1-4% compared to that of well-fed cultures. All cultures in Bioassays 1 and 2 were incubated at 28°C, and with vigorous stirring (650 rpm). Results from experiments using Bioassay 1 are presented in Figs. 5 and S2.

FIG 2 Denitrification kinetics as affected by starvation in cultures with a complete denitrification proteome (Bioassay 1). Cells were allowed to develop a full denitrification proteome under well-fed conditions and were then washed twice in buffer prior to inoculation to flasks with YMB (well-fed control) or buffer (starved), supplemented with 1 mM KNO_3 and 0.25 mM KNO_2, and with He plus 1 ml N_2O (around 80 µmol N) in headspace. A larger inoculum was given to the flasks with buffer (9.9E+08 cells $flask^{-1}$) than to the flasks with YMB (5.0E+09 cells $flask^{-1}$), to secure measurable activity in the starved cells and adequate time resolution of the denitrification kinetics in the well-fed cells. Panels A and B show the denitrification kinetics in well-fed and starved cultures, respectively. The flasks were practically anoxic from the start with an initial O_2 concentration in the liquid of <0.52 µM which decreased to approximately 0 µM (insets in A & B). Panels C and D show the cell specific electron flow rate. $V_{e\ total\ den}$ designates the total electron flow to the denitrification reductases and $V_{e\ total\ incl\ O2}$ the total electron flow, including that to denitrification and to O_2. The electron flow rate to the individual reductases is designated as V_{eNap}, V_{eNir}, V_{eNor} and V_{eNos}. V_{eNir} and V_{eNor} were practically identical and cannot be distinguished from one another in the figure. Inserted panels show V_{eNap} throughout, including negative values which are due to slight errors in determination of N_2 and N_2O (V_{eNap} was calculated by N-mass balance). Bars in all graphs show standard deviation (n=3).

FIG 3 Bioassay 1 with single nitrogen oxides**.** Experimental conditions as for Fig. 2, but the starving cells (in buffer) were provided with either NO_3^-, NO_2^- or N_2O in individual flasks (n=3 for each treatment). Panels A-C show the gas kinetics in flasks provided with 1 mM NO_3^- (A), 0.5 mM NO_2^- (B), or 70 µmol N_2O-N added to the headspace (C). Panel D shows the cell-specific

742 electron flow rate (V_e) measured in buffer supplemented with NO_3^-, NO_2^- or N_2O; the O_2
743 concentration (left y-axis); and V_e as percentage of the rates in well-fed cultures (right y-axis).
744 The number of cells inoculated into the incubation flasks at the start (0 h of incubation in anoxic
745 buffer) was 3.6E+09 for all treatments. Bars show standard deviation (n=3).
746
747 **FIG 4** Denitrification in starved cells after addition of TMPD as an external electron donor.
748 Preparation of the cultures followed Bioassay 1 (Fig. 1A), except that 100 µM TMPD and 10 mM
749 ascorbate were injected into the flasks with starving cells 15 min before the first gas sampling.
750 Each flask was inoculated with 5.28E+08 cells (n=4 replicate flasks). The initial O_2 concentration
751 was 0.35 µM and decreased to approximately 0 within 5 h (inset in A). Bars show standard
752 deviation (n=4). Panel A: kinetics of NO_2^-, NO, N_2O and N_2 (O_2 in inserted panel). Panel B:
753 Calculated cell specific electron flow rate (V_e, fmol $cell^{-1}$ h^{-1}) to each of the reductases Nap, Nir,
754 Nor, and NosZ, and the total electron flow rate (V_{etotal}). The electron flow to Nir was practically
755 identical to the electron flow to Nor (miniscule amounts of NO), and the two are shown as a
756 single graph ($V_{eNir/Nor}$). Inset plots show V_{eNap} throughout, including negative values which are
757 due to slight errors in determination of N_2 and N_2O (V_{eNap} was calculated by N-mass balance).
758
759 **FIG 5** Bioassay 2: stochasticity of starvation response, response to input of organic C and
760 quantification of denitrification enzymes. Altogether fifteen flasks were prepared following
761 Bioassay 2 (see Fig. 1B). All flasks were anoxic (<0.5 µM at the start of the incubation) and
762 contained 50 ml buffer supplemented with 1 mM KNO_3 and with He plus 1 ml N_2O in the
763 headspace. The NO_2^- concentrations, measured during the first 5 hours after incubation in the

764 buffer, were approximately 0.59±0.20 µM (not shown). The cultures separated into two distinct
765 phenotypes: nine flasks had “slow” respiration (panel A) and 6 flasks had “fast” respiration
766 (panel B). The electron flow to the individual reductases (fmol e^- $cell^{-1}$ h^{-1}) for the flasks with
767 slow and fast respiration are shown in panels C and D, respectively. Cultures with “slow”
768 respiration rate had a total electron flow rate of maximum 0.27 e^- $cell^{-1}$ h^{-1} (C) and cultures with
769 “fast” respiration rate had a total electron flow rate of 1.0-1.8 fmol e- $cell^{-1}$ h^{-1} (D). The inset plot
770 in panel C shows the electron flow to the individual denitrification reductases after the carbon
771 addition. The cultures (entire flasks, 50 ml) were sampled for proteomics analyses at different
772 time points (panels E and F). At timepoints throughout, marked by dashed vertical lines in
773 panels A and B, three flasks were harvested for proteomics analysis (including 0 h). The six flasks
774 with “fast” respiration were harvested for proteomics analysis at 5 and 20 h of incubation in
775 these anoxic buffers (triplicates at each sampling point). Of the nine flasks with “slow”
776 respiration, three were harvested at 10 and three at 20 h. The remaining three “slow”
777 respiration flasks were supplemented with YMB at 24.8 h, at a concentration which made the
778 buffer a half-strength YMB medium, containing 5 g mannitol l^{-1} and 0.25 yeast extract l^{-1}, and
779 then harvested for proteomics at 27 h. The gas measurements and electron flows are averages
780 from the three flasks (n=3) for each phenotype, that were left untouched until the end of the
781 incubation when they were sampled for proteomics. Proteomics analyses were done for
782 triplicate flasks (n=3) at each sampling point. Standard deviations are indicated as bars in all
783 graphs (in several cases not visible due to low variation).
784

Bioassay 1: Denitrification induced before starvation

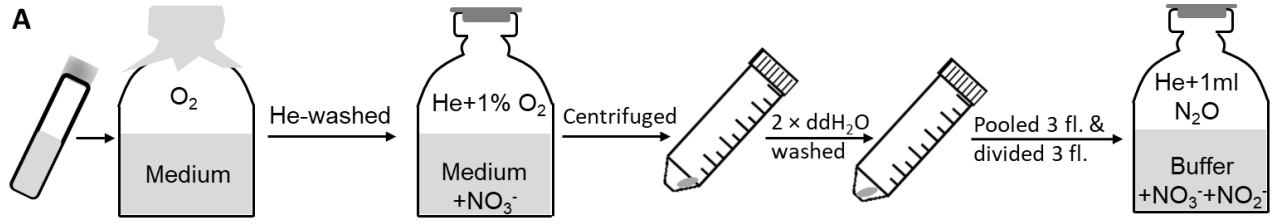

Bioassay 2: Denitrification induced during starvation

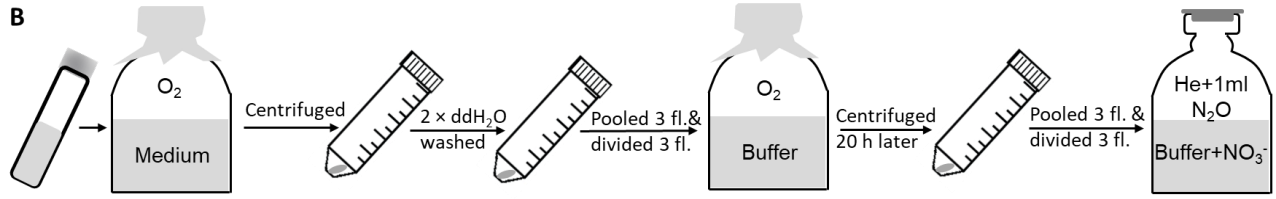

FIG 1 Bioassays for assessing the effect of starvation on electron flow to denitrification enzymes.
A: Bioassay 1: starvation of cells with a previously expressed denitrification proteome. Cells were raised from stock cultures in fully oxic flasks containing YMB medium. When OD_{600} reached ~0.1, the flasks were made anoxic by He-washing, then supplemented with 1% O_2 in the headspace and 1 mM NO_3^- in the liquid. The cultures were allowed to deplete the O_2 and to initiate denitrification when growing in YMB medium, after which they were centrifuged (10 000 × g at 4 °C for 10 mins) and washed twice in sterile ddH_2O. The pellets from triplicate flasks were pooled and used to inoculate flasks containing either C-free buffer or YMB medium (well-fed control), in both cases supplemented with 1 mM KNO_3 and 0.25 or 0.5 mM KNO_2, and with He and 1 ml N_2O (around 80 µmol N $flask^{-1}$) in headspace. The starving cells, incubated in buffer, had a low respiratory electron flow rate (mol electrons $cell^{-1}$ h^{-1}), initially being 10-18 % that of the well-fed cultures, and then decreasing to reach around 4% after 20 h. Results from experiments using Bioassay 1 are presented in Figs. 2, 3 and 4.
B: Bioassay 2: denitrification induced during starvation. Cells were raised from stock cultures in fully oxic flasks containing YMB medium. When OD_{600} reached ~0.1, the cultures were centrifuged (10 000 × g at 4 °C for 10 mins) and washed twice in sterile ddH_2O. The pellets from triplicate flasks were pooled, after which they were evenly divided and used to inoculate fully oxic flasks containing C-free buffer. These cultures were incubated for 20 h, then centrifuged after which the pellets were pooled and divided evenly before being inoculated into flasks containing C-free buffer-provided with 1 mM KNO_3, and with He and 1 ml N_2O (around 80 µmol N $flask^{-1}$) in headspace. The respiration rate (mol electrons $cell^{-1}$ h^{-1}) of the starving cultures was 1-4% compared to that of well-fed cultures. All cultures in Bioassays 1 and 2 were incubated at 28°C, and with vigorous stirring (650 rpm). Results from experiments using Bioassay 1 are presented in Figs. 5 and S2.

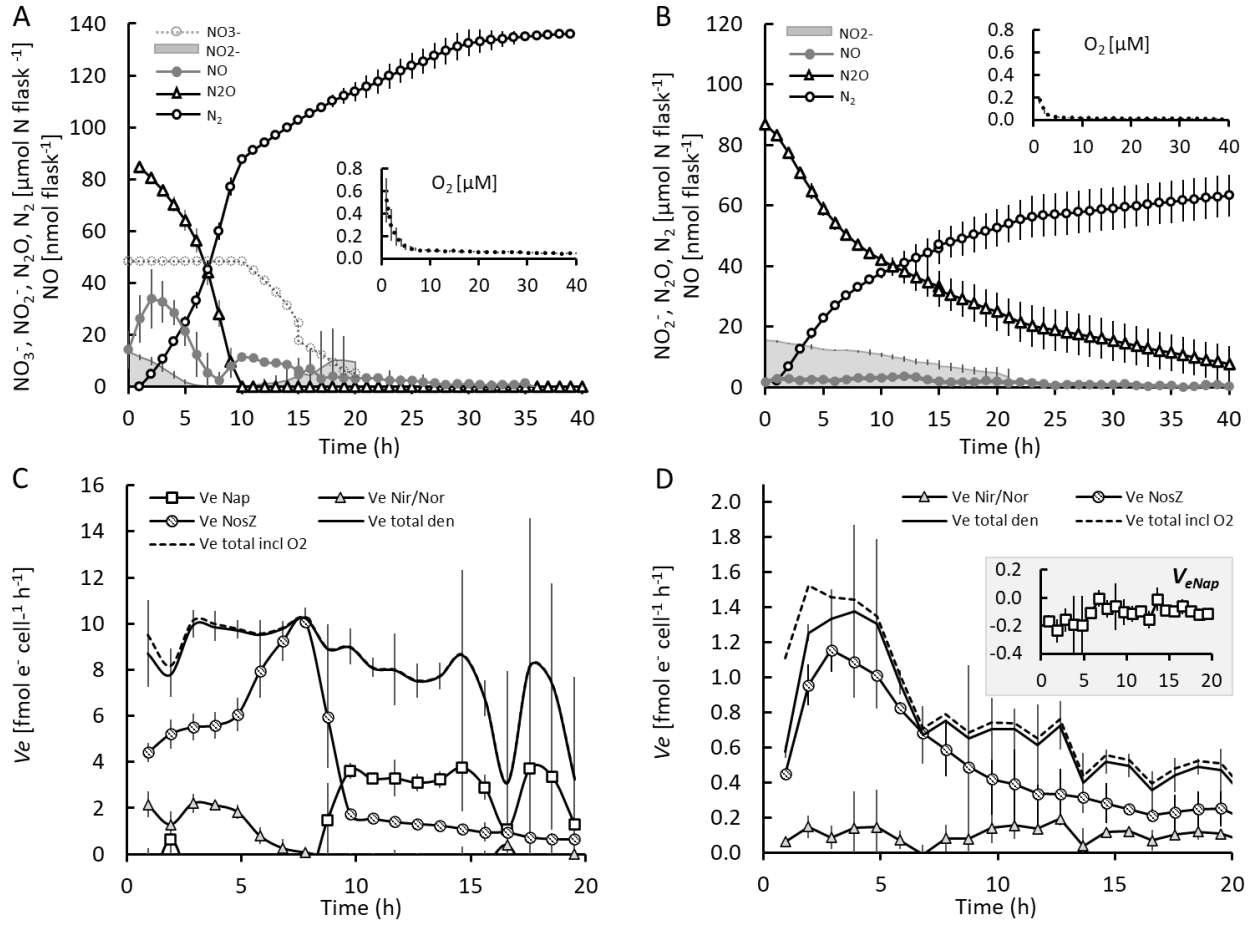

FIG 2 Denitrification kinetics as affected by starvation in cultures with a complete denitrification proteome (Bioassay 1). Cells were allowed to develop a full denitrification proteome under well-fed conditions and were then washed twice in buffer prior to inoculation to flasks with YMB (well-fed control) or buffer (starved), supplemented with 1 mM KNO_3 and 0.25 mM KNO_2, and with He plus 1 ml N_2O (around 80 µmol N) in headspace. A larger inoculum was given to the flasks with buffer (9.9E+08 cells flask^{-1}) than to the flasks with YMB (5.0E+09 cells flask^{-1}), to secure measurable activity in the starved cells and adequate time resolution of the denitrification kinetics in the well-fed cells. Panels A and B show the denitrification kinetics in well-fed and starved cultures, respectively. The flasks were practically anoxic from the start with an initial O_2 concentration in the liquid of <0.52 µM which decreased to approximately 0 µM (insets in A & B). Panels C and D show the cell specific electron flow rate. $V_{e\ total\ den}$ designates the total electron flow to the denitrification reductases and $V_{e\ total\ incl\ O2}$ the total electron flow, including that to denitrification and to O_2. The electron flow rate to the individual reductases is designated as V_{eNap}, V_{eNir}, V_{eNor} and V_{eNos}. V_{eNir} and V_{eNor} were practically identical and cannot be distinguished from one another in the figure. Inserted panels show V_{eNap} throughout, including negative values which are due to slight errors in determination of N_2 and N_2O (V_{eNap} was calculated by N-mass balance). Bars in all graphs show standard deviation (n=3).

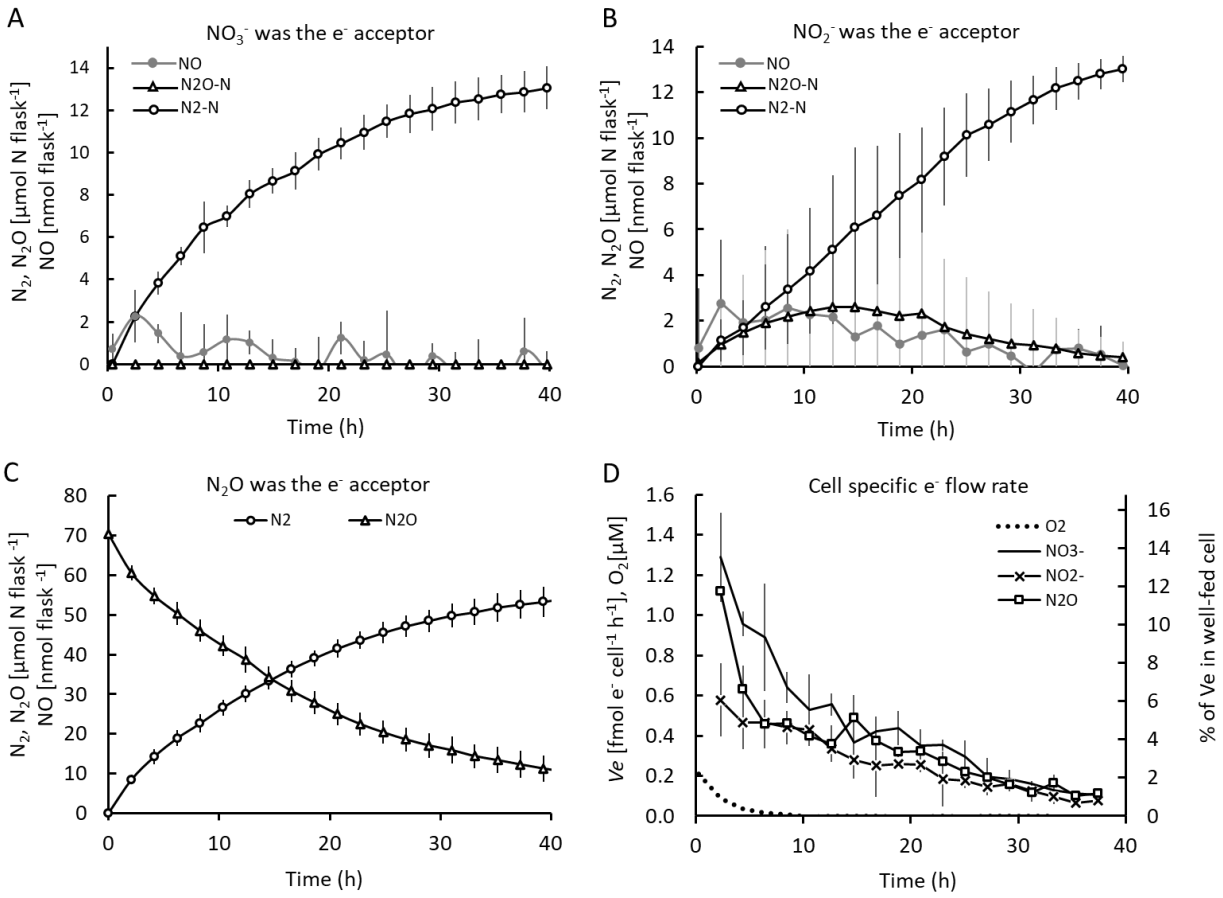

FIG 3 Bioassay 1 with single nitrogen oxides**.** Experimental conditions as for Fig. 2, but the starving cells (in buffer) were provided with either NO_3^-, NO_2^- or N_2O in individual flasks (n=3 for each treatment). Panels A-C show the gas kinetics in flasks provided with 1 mM NO_3^- (A), 0.5 mM NO_2^- (B), or 70 µmol N_2O-N added to the headspace (C). Panel D shows the cell-specific electron flow rate (V_e) measured in buffer supplemented with NO_3^-, NO_2^- or N_2O; the O_2 concentration (left y-axis); and V_e as percentage of the rates in well-fed cultures (right y-axis). The number of cells inoculated into the incubation flasks at the start (0 h of incubation in anoxic buffer) was 3.6E+09 for all treatments. Bars show standard deviation (n=3).

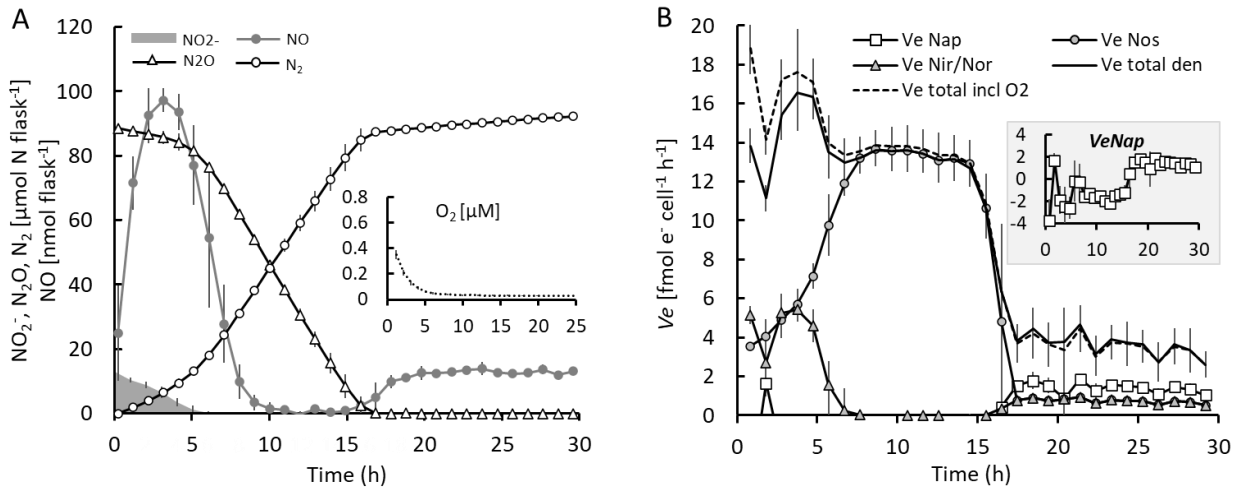

FIG 4 Denitrification in starved cells after addition of TMPD as an external electron donor. Preparation of the cultures followed Bioassay 1 (Fig. 1A), except that 100 µM TMPD and 10 mM ascorbate were injected into the flasks with starving cells 15 min before the first gas sampling. Each flask was inoculated with 5.28E+08 cells (n=4 replicate flasks). The initial O_2 concentration was 0.35 µM and decreased to approximately 0 within 5 h (inset in A). Bars show standard deviation (n=4). Panel A: kinetics of NO_2^-, NO, N_2O and N_2 (O_2 in inserted panel). Panel B: Calculated cell specific electron flow rate (V_e, fmol cell^{-1} h^{-1}) to each of the reductases Nap, Nir, Nor, and NosZ, and the total electron flow rate (V_{etotal}). The electron flow to Nir was practically identical to the electron flow to Nor (miniscule amounts of NO), and the two are shown as a single graph ($V_{eNir/Nor}$). Inset plots show V_{eNap} throughout, including negative values which are due to slight errors in determination of N_2 and N_2O (V_{eNap} was calculated by N-mass balance).

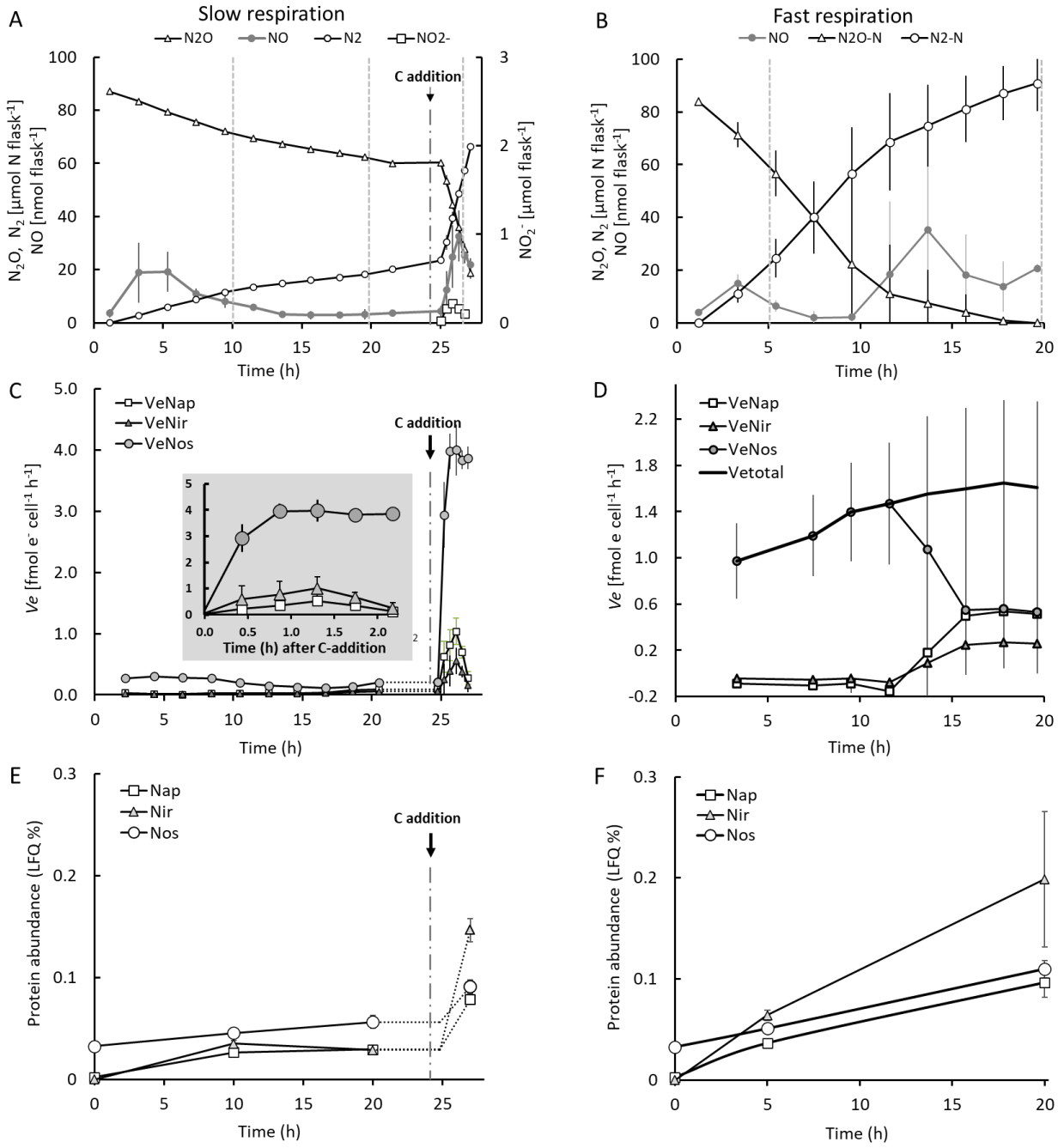

FIG 5 Bioassay 2: stochasticity of starvation response, response to input of organic C and quantification of denitrification enzymes. Altogether fifteen flasks were prepared following Bioassay 2 (see Fig. 1B). All flasks were anoxic (<0.5 µM at the start of the incubation) and contained 50 ml buffer supplemented with 1 mM KNO_3 and with He plus 1 ml N_2O in the headspace. The NO_2^- concentrations, measured during the first 5 hours after incubation in the buffer, were approximately 0.59±0.20 µM (not shown). The cultures separated into two distinct phenotypes: nine flasks had "slow" respiration (panel A) and 6 flasks had "fast" respiration (panel B). The electron flow to the individual reductases (fmol e^- $cell^{-1}$ h^{-1}) for the flasks with slow and fast respiration are shown in panels C and D, respectively. Cultures with "slow" respiration rate had a total electron flow rate of maximum 0.27 e^- $cell^{-1}$ h^{-1} (C) and cultures with "fast" respiration rate had

a total electron flow rate of 1.0-1.8 fmol e- $cell^{-1}$ h^{-1} (D). The inset plot in panel C shows the electron flow to the individual denitrification reductases after the carbon addition. The cultures (entire flasks, 50 ml) were sampled for proteomics analyses at different time points (panels E and F). At timepoints throughout, marked by dashed vertical lines in panels A and B, three flasks were harvested for proteomics analysis (including 0 h). The six flasks with "fast" respiration were harvested for proteomics analysis at 5 and 20 h of incubation in these anoxic buffers (triplicates at each sampling point). Of the nine flasks with "slow" respiration, three were harvested at 10 and three at 20 h. The remaining three "slow" respiration flasks were supplemented with YMB at 24.8 h, at a concentration which made the buffer a half-strength YMB medium, containing 5 g mannitol l^{-1} and 0.25 yeast extract l^{-1}, and then harvested for proteomics at 27 h. The gas measurements and electron flows are averages from the three flasks (n=3) for each phenotype, that were left untouched until the end of the incubation when they were sampled for proteomics. Proteomics analyses were done for triplicate flasks (n=3) at each sampling point. Standard deviations are indicated as bars in all graphs (in several cases not visible due to low variation).